

# Feedforward Excitation and Inhibition Evoke Dual Modes of Firing in the Cat's Visual Thalamus during Naturalistic Viewing

Xin Wang,<sup>1</sup> Yichun Wei,<sup>1</sup> Vishal Vaingankar,<sup>1</sup> Qingbo Wang,<sup>2</sup> Kilian Koepsell,<sup>3</sup> Friedrich T. Sommer,<sup>3</sup> and Judith A. Hirsch<sup>1,2,\*</sup>

<sup>1</sup>Neuroscience Graduate Program

<sup>2</sup>Department of Biological Sciences

University of Southern California, 3641 Watt Way, Los Angeles, CA 90089-2520, USA

<sup>3</sup>Redwood Center for Theoretical Neuroscience, University of California, Berkeley, 132 Barker, Berkeley, CA 94720-3190, USA

\*Correspondence: [jhirsch@usc.edu](mailto:jhirsch@usc.edu)

DOI 10.1016/j.neuron.2007.06.039

## SUMMARY

Thalamic relay cells transmit information from retina to cortex by firing either rapid bursts or tonic trains of spikes. Bursts occur when the membrane voltage is low, as during sleep, because they depend on channels that cannot respond to excitatory input unless they are primed by strong hyperpolarization. Cells fire tonically when depolarized, as during waking. Thus, mode of firing is usually associated with behavioral state. Growing evidence, however, suggests that sensory processing involves both burst and tonic spikes. To ask if visually evoked synaptic responses induce each type of firing, we recorded intracellular responses to natural movies from relay cells and developed methods to map the receptive fields of the excitation and inhibition that the images evoked. In addition to tonic spikes, the movies routinely elicited lasting inhibition from the center of the receptive field that permitted bursts to fire. Therefore, naturally evoked patterns of synaptic input engage dual modes of firing.

## INTRODUCTION

Thalamic relay cells determine how input from the eye is transmitted to cortex. The pattern of activity that these neurons send downstream depends strongly on the level of membrane polarization. When the membrane rests at depolarized levels, relay cells produce tonic trains of action potentials, but when the membrane is hyperpolarized, they fire rapid bursts. The bursts are initiated by calcium channels that open transiently at voltages below spike threshold and remain inactivated until exposed to substantial hyperpolarization (Jahnsen and Llinas, 1984). Early recordings made from unanaesthetized animals suggested that the tonic mode of firing was associated with

wakefulness, and the burst mode with drowsiness or sleep (Fourment et al., 1984; Livingstone and Hubel, 1981; Steriade et al., 1993). Recent work, however, indicates that firing mode is not strictly linked to behavioral state (Denning and Reinagel, 2005; Guido et al., 1992; Lesica and Stanley, 2004; Ramcharan et al., 2000; Reinagel and Reid, 2000; Swadlow and Gusev, 2001; Wolfart et al., 2005). Bursts, though not common, occur routinely in awake animals and can be evoked by sensory stimuli (Guido et al., 1992; Ramcharan et al., 2000; Swadlow and Gusev, 2001; Weyand et al., 2001). The possibility that bursts contribute to normal sensory function is important. For example, the temporal pattern of spike trains determines the amount and type of information that can be encoded about the stimulus (Denning and Reinagel, 2005; Liu et al., 2001; Reinagel et al., 1999). Further, bursts activate the cortex more effectively than slower trains of spikes (Swadlow and Gusev, 2001; Swadlow et al., 2002), likely because they evoke synaptic potentials that summate in time (Usrey et al., 2000), and also because they occur after long silences that permit recovery from synaptic depression (Swadlow and Gusev, 2001; Swadlow et al., 2002).

Extracellular studies have shown that visually evoked bursts are most likely to occur after prolonged exposure to nonpreferred stimuli (Alitto et al., 2005; Denning and Reinagel, 2005; Lesica and Stanley, 2004). These findings suggest that lasting and suppressive stimuli somehow evoke hyperpolarizations strong enough to revive the calcium channels that trigger thalamic bursting (Alitto et al., 2005; Denning and Reinagel, 2005; Lesica and Stanley, 2004). To explore the intracellular mechanisms that might prime bursts during vision, we made whole-cell recordings in vivo. To lay the foundation for our study, we explored the synaptic basis of the thalamic receptive field. Tests with simple visual patterns revealed that relay cells had receptive fields in whose On and Off subregions stimuli of the reverse contrast evoke synaptic responses of the opposite sign, an arrangement called push-pull. Since both the excitatory and inhibitory contributions to the receptive field had the center-surround structure

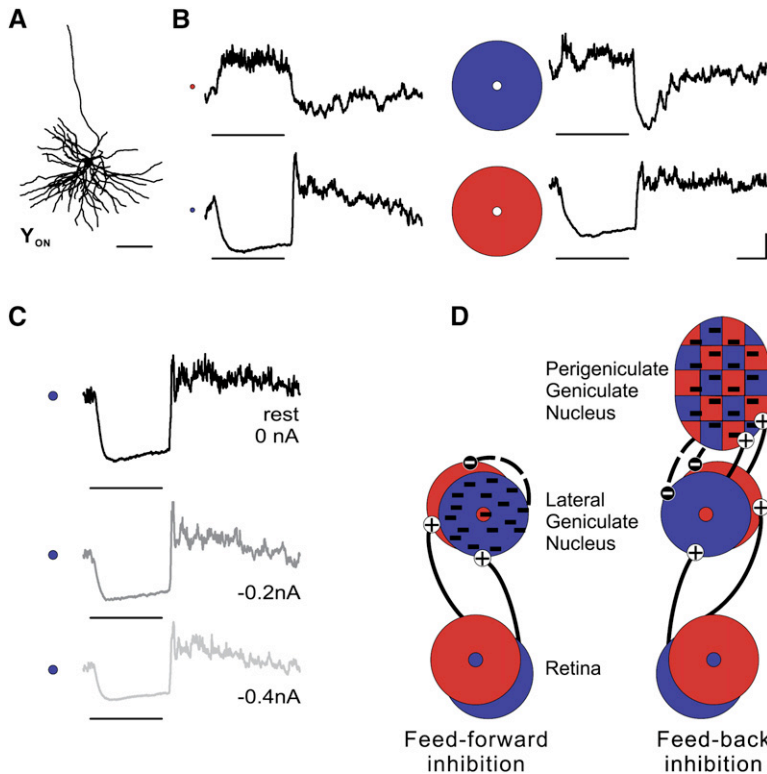


**Figure 1. Spatially Opponent Excitation, or Push, and Inhibition, or Pull, in the Relay Cell's Receptive Field**

(A) Anatomical reconstruction of an On center Y cell in layer A1; scale bar, 100  $\mu\text{m}$ .

(B) Averaged responses to ten trials of bright (red) and dark (blue) disks and annuli in the receptive field center and surround; disk size  $1^\circ$ , annulus size  $2^\circ$ ,  $20^\circ$ ; horizontal bars under the traces mark stimulus duration; scale bars are 10mV and 200 ms in this and the following panel.

(C) Voltage dependence of the hyperpolarization evoked by suppressive stimuli; response recorded at different holding currents:  $-0.2$  nA (dark gray line), 0 nA (black line),  $-0.2$  nA,  $-0.4$  nA (light gray line).

(D) Wiring diagram for feedforward, push-pull responses mediated by local interneurons (left) and for feedback inhibition from the perigeniculate nucleus (right). Cells are represented as their receptive fields; blue indicates Off subregions; red, On subregions; and minus signs, interneurons; solid and dashed lines indicate excitatory and inhibitory connections, respectively. Drawings of overlapping On and Off receptive fields in the retina and the lateral geniculate nucleus are offset in the figure for the purpose of illustration.

characteristic of ganglion cells, we concluded that feedforward circuits give rise to both push and pull. Further, we observed that lasting stimuli of the nonpreferred contrast evoked strong inhibition that enabled bursts. This result recalled ecological viewing conditions: in nature, light levels within the receptive field can remain steady for long durations (Denning and Reinagel, 2005; Dong and Atick, 1995). Thus, it seemed reasonable to suppose that synaptic responses to time-varying natural images (i.e. movies) could drive the membrane between tonic and burst modes. Our recordings confirmed this prediction. We next devised methods to map the spatiotemporal organization of the excitation and inhibition the movies evoked to learn how response pattern relates to receptive field structure and, by inference, underlying circuitry. Our results lead to a simple conclusion: retinogeniculate (or feedforward) inhibition driven from the center of the receptive field is sufficient to prime bursts for all types of relay cells.

## RESULTS

To explore how visually evoked synaptic input influences firing pattern, we made whole-cell recordings from 42 relay cells in 12 adult cats. We recorded from all layers (A, A1, and C) of the lateral geniculate and were able to classify 20 cells, including X cells ( $n = 9$ ), Y cells ( $n = 8$ ), and W cells ( $n = 3$ ), by anatomical criteria (Friedlander et al., 1981).

## Synaptic Structure of Thalamic Receptive Fields

Extracellular recordings have shown that thalamic relay cells, like retinal ganglion cells, have circular receptive fields made of two concentric subregions that have the opposite preference for stimulus contrast: bright stimuli falling within On subregions evoke firing, as do dark stimuli shown within Off subregions (Wiesel, 1959). We made whole-cell recordings of responses to classical stimuli, disks and annuli, to map the dominant patterns of excitatory and inhibitory input to the thalamic receptive fields. Our intracellular analyses showed that within each subregion, stimuli of the reverse contrast evoke responses of the opposite sign—a push-pull profile. For example, a bright disk flashed in the On center of a Y cell (Figure 1A) evoked a depolarization (push) (Figure 1B, top left), whereas a dark disk of the same size and position evoked a strong hyperpolarization (pull) (Figure 1B, bottom left). Rebound responses of the opposite sign followed the withdrawal of the stimulus; traces are averages of ten trials. A similar pattern was elicited by annuli presented to the surround (Figure 1B, right). To determine if the pull (stimulus-evoked hyperpolarization) was caused by synaptic inhibition versus withdrawal of excitatory drive, we made recordings when the membrane potential was lowered by means of current injection. The amplitude of the response diminished with progressive hyperpolarization (Figure 1C,  $n = 4$  cells). These results suggest that the pull was dominated by GABAergic currents, which reverse below the resting membrane potential (Crunelli et al., 1988). Note that a hyperpolarization resulting from withdrawal

of excitation would have had the opposite voltage dependence; it would have increased in amplitude when the membrane potential was made more negative.

A simple circuit that might explain the responses we recorded is illustrated in [Figure 1D](#) (left). The excitation, or push, is created by ganglion cells whose receptive fields have the same position and center sign as the relay cell. The inhibition, or pull, is generated by interneurons supplied by ganglion cells whose receptive fields share the same position but have the opposite sign as the relay cell. There is, in fact, evidence that interneurons in the main layers of the lateral geniculate nucleus have center-surround receptive fields ([Humphrey and Weller, 1988](#); [Sherman and Friedlander, 1988](#)). By contrast, the inhibition we recorded was unlikely to be structured by input from the overlying perigeniculate nucleus, which receives input from relay cells en route to cortex and feeds back inhibition to the lateral geniculate. Receptive fields in the perigeniculate are usually large, irregularly shaped, and have overlapping On and Off responses ([Dubin and Cleland, 1977](#); [Uhrlich et al., 1991](#); [Wörgötter et al., 1998](#)); see [Figure 1D](#), right.

#### Tonic and Burst Firing Mode in Response to Naturalistic Stimulation

In order to understand how the structure of the receptive field influences neural output under ecological viewing conditions, we recorded responses evoked by various natural movies, as illustrated for an Off center X cell in [Figure 2A](#). Insets at top in [Figure 2B](#) show frames of a movie of windblown tree branches in which the luminance of the patch that fell within the center of the receptive field ([Figure 2C](#)) was variously brighter or darker. Intracellular responses to repeated clips of the natural movie show that the stimulus evoked a broad but reproducible range of behaviors that included both tonic and burst firing. Responses recorded in current-clamp mode ([Figure 2D](#)) are shown above those recorded in voltage-clamp mode ([Figure 2E](#)). Voltage-clamp mode mildly damped the membrane currents. Thus, strong depolarizing currents that evoked bursts and spikes remained robust, but small fluctuations in the shapes of individual synaptic events were reduced such that excitatory postsynaptic currents (EPSCs) could be reliably detected and analyzed. When the frames of the movie are compared to the recordings, one sees that darker patterns that fell over the center of the receptive field evoked high rates of synaptic input and tonic firing, whereas brighter patterns led to hyperpolarizing responses. Moreover, the transition from lasting brightness to darkness was accompanied by bursts of spikes on top of the slow depolarizing waveform ([Figures 2D](#) and [2E](#)). This sequence, in which bursts marked the end of prolonged exposure of the center of the receptive field to a stimulus of the nonpreferred contrast, was common in our sample and has been reported in extracellular studies ([Alitto et al., 2005](#); [Lesica et al., 2006](#)). Similar results were found when the movies were shown through a central aperture within the receptive field center ( $n = 2$ , not shown), suggesting that most

of the response we observed was mediated from the center versus the surround of the receptive field. Further, disks of the nonpreferred contrast flashed in the center of the receptive field also evoked inhibition that primed bursts ([Figure 2G](#)).

#### Mapping Receptive Fields from Responses to Natural Movies

In order to understand the responses to natural movies in terms of the contributions from different regions of visual space, we developed means to extract the receptive fields of the inputs, excitatory and inhibitory synaptic currents, and the outputs, spikes. The initial step was to separate the different components of the response. Unitary events, namely, the excitatory synaptic inputs and spikes, were sorted on the basis of peak amplitude and maximum slope. The inhibitory part of the response could not be obtained in the same fashion because individual inhibitory postsynaptic currents (IPSCs) were not visible; rather, they pooled to form graded currents. Thus, our approach was to extract the inhibitory component by removing the excitatory events from the intracellular signal. First, we constructed a record in which each spike ([Figure 2F](#), top) and EPSC ([Figure 2F](#), middle) was represented by a template of the average event in each class. We then subtracted those simulated waveforms from the raw record (see [Experimental Procedures](#)). The residual signal ([Figure 2F](#), bottom) consisted almost entirely of the hyperpolarizing responses, albeit with a small contribution from unclamped inward currents like those that drove bursts ([Figure 2F](#), asterisk). These inward bumps under the bursts most likely resulted from low-threshold calcium currents (T-currents) ([Jahnsen and Llinas, 1984](#)), possibly with modest contributions from glutamate receptors ([Blitz and Regehr, 2003](#)) or rapid trains of retinal input ([Sincich et al., 2007](#)) masked by intrinsic conductances. As a control for the above method of isolating inhibition, we subtracted records made at membrane levels negative to the holding level and found similar results ( $n = 2$ ; see [Figure S1](#) in the [Supplemental Data](#) available with this article online).

The next step was to map the receptive fields of the different components of the responses to movies. To accomplish this task the intrinsic spatial and temporal correlations in the movies ([Dong and Atick, 1995](#)) had to be taken into account. The approach we used was to obtain the receptive fields by finding the spatiotemporal kernel that best predicted the actual neural response (see [Experimental Procedures](#)). Although the method yields only the linear component of the response, the predictions fit the data quite well, as expected from previous analyses of thalamic spike trains ([Dan et al., 1996](#); [Mante et al., 2005](#)). Further, we checked the reconstructions made from the natural stimuli against receptive fields mapped conventionally by sparse or dense noise and found similar patterns of push and pull for all stimulus conditions (see [Experimental Procedures](#)). The responses to the movies were dominated by excitation and inhibition evoked from the center of the receptive field, as illustrated

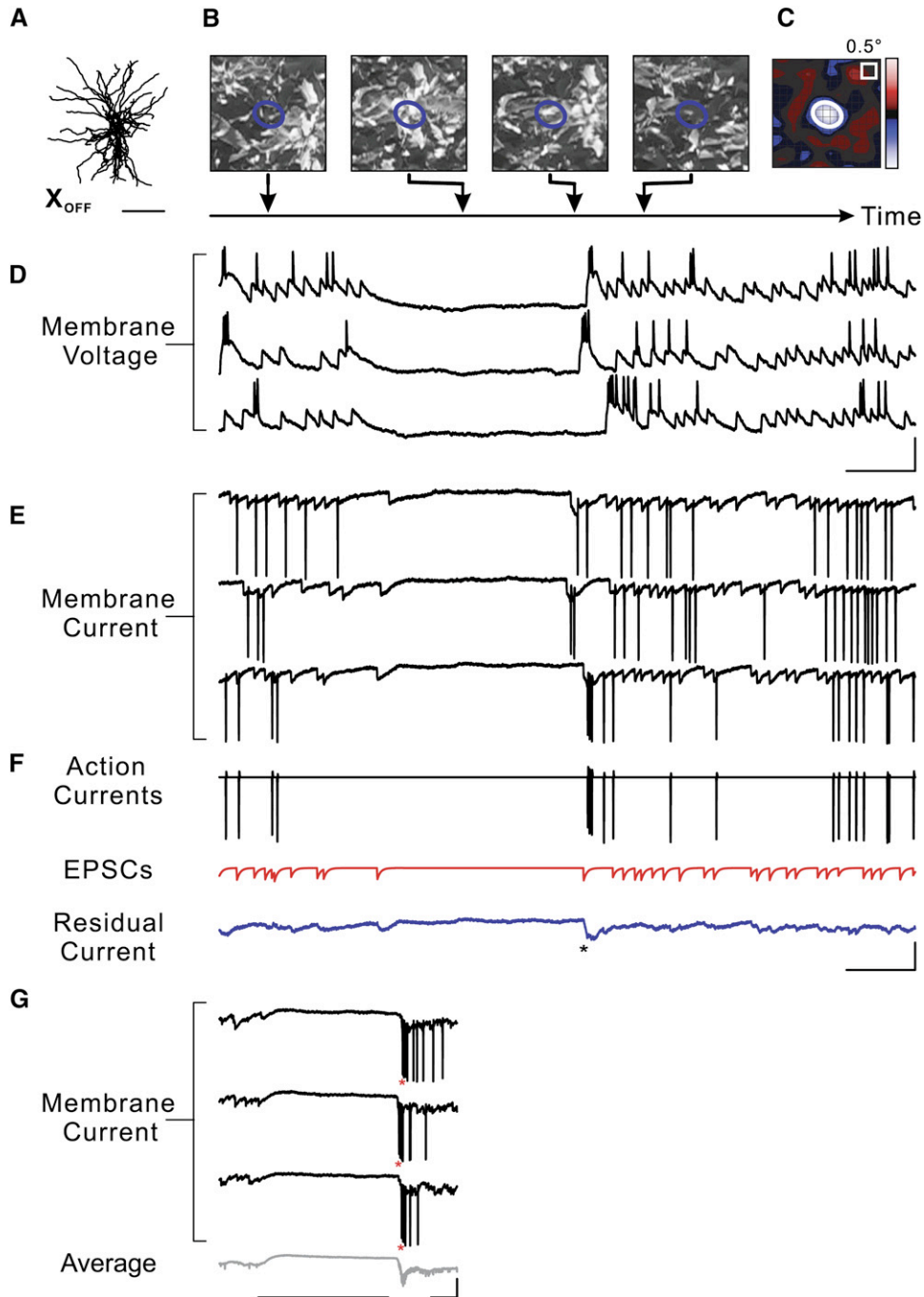


**Figure 2. Intracellular Responses of a Relay Cell to Repeated Presentations of Natural Movies**

(A) Anatomical reconstruction of an Off center X cell in layer A; scale bar, 100  $\mu$ m.

(B) Insets show examples of movie frames that introduced marked changes in luminance in the receptive field center (blue ellipse); arrows point to the time at which each frame appeared.

(C) Receptive field of the retinal input reconstructed from responses to repeated presentations of the movie; white ellipse is the  $1.5\sigma$  contour from a 2D Gaussian fit.

(D) Clips of responses to three presentations of the movie recorded in current-clamp mode; scale bars, 200 ms and 10mV.

(E) Responses to the same segment of the movie recorded in voltage-clamp mode, which damped intrinsic conductances.

(F) Separation of components of the raw data, as illustrated for the lowest trace in (E). The black trace shows spikes, the red trace shows templates fit to each EPSC, and the blue trace shows the residual (spike and EPSC subtracted) currents, which were mainly hyperpolarizing but also contained occasional putative T-currents (asterisk); scale bars, 200 ms and 100 pA.

for morphologically identified X, Y, and W relay cells of both center signs. Anatomical reconstructions (Figure 3A) are shown above the receptive fields for push (EPSCs) (Figure 3B, top); for pull (inhibition) (Figure 3B, middle); and for spikes (Figure 3B, bottom; white ovals mark 2D Gaussian fits of the center). The temporal pattern of response for each component is shown in Figure 3C.

It seemed logical to think that the excitatory postsynaptic events came from retina; there is general consensus that feedforward input shapes the relay cell's receptive field (Cleland et al., 1971; Levick et al., 1972; Usrey et al., 1999). By contrast, intracellular studies in vitro show that corticogeniculate EPSC inputs are difficult to detect (Granseth and Lindstrom, 2003), as is consistent with their origin on distal dendrites (Sherman and Guillery, 1996). We further reasoned that if the shape of the pull evoked by the movies resembled that of the push, then the pull was likely to arise from feedforward retinal input relayed via local interneurons rather than from feedback from the perigeniculate (see Figure 1D). Thus, we quantified the similarity between the push and pull using several measures detailed below.

First we adapted Schiller's overlap index (Schiller et al., 1976) (see Experimental Procedures) to measure the extent of overlap between the push and pull in the central subregion of the receptive field. The index gives a value of 1 for cospatial subregions and a value of 0 for subregions that lie side by side. The score for the entire population was high,  $0.720 \pm 0.022$  ( $n = 41$ ), indicating a high degree of overlap (Martinez et al., 2005). Scores within different classes of cells were similar (Figure 3D, top histogram: X cells,  $0.740 \pm 0.025$ ,  $n = 9$ ; Y cells,  $0.761 \pm 0.033$ ,  $n = 8$ ; W cells,  $0.787 \pm 0.025$ ,  $n = 3$ ; unlabeled cells,  $0.686 \pm 0.038$ ,  $n = 21$ ). Next, we asked whether the pull and push were similar in size by calculating the ratio of their center areas. The value of the pull-push ratio was  $1.00 \pm 0.04$  ( $n = 41$ ) for the whole sample (Figure 3D, right histogram). The ratios within classes were  $0.87 \pm 0.08$  (X cells,  $n = 9$ ),  $1.01 \pm 0.06$  (Y cells,  $n = 8$ ),  $0.93 \pm 0.09$  (W cells,  $n = 3$ ) and  $1.05 \pm 0.07$  (unlabeled cells,  $n = 21$ ). A plot of the overlap index against the pull-push ratio illustrates that the push and pull usually overlapped and were of comparable area; the colored crosses are centered on the population mean and mark the standard deviation (Figure 3D). Last, we asked if the shape of the pull was as round as that of retinal input by using an index of elliptical eccentricity for which 0 indicates circular symmetry and values that approach 1 indicate progressively ovoid shapes. The values for X cells were  $0.61 \pm 0.05$  for push and  $0.65 \pm 0.03$  for pull ( $n = 9$ ); for Y cells,  $0.54 \pm 0.05$  for push and  $0.63 \pm 0.05$  for pull ( $n = 8$ ); for W cells,  $0.72 \pm 0.08$  for push and  $0.83 \pm 0.02$  for pull ( $n = 3$ ); and for unlabeled cells,  $0.60 \pm 0.03$  for push and  $0.61 \pm 0.04$  for pull ( $n = 21$ ). Values for the entire sample were  $0.60 \pm 0.02$

( $n = 41$ ) for push and  $0.64 \pm 0.02$  ( $n = 41$ ) for pull. Although the degree of elongation of the receptive fields varied somewhat, as reported for retinal ganglion cells (Shou et al., 1986), the push and pull had similar geometries (see Experimental Procedures; Figure 3E). In sum, all three indices are consistent with a feedforward origin of the pull.

The overlap indices between push and pull that we measured here (and see Martinez et al., 2005) are consistent with predictions based on the anatomical layout of On and Off ganglion cells in the retinal mosaic (Wässle et al., 1981) and the spatial extents of ganglion cells' receptive fields (Peichl and Wässle, 1983). Specifically, the mean value we calculate from our data, 0.72, and the value we calculate based on studies of the retinal mosaic, 0.70, are similar (see Supplement). Of course, other features could influence the relative overlap between push and pull, such as convergence and divergence in the retinogeniculate connectivity (Hamos et al., 1987).

### Feedforward Inhibition Primes Bursts

Visual inspection of our records had suggested that long periods of inhibition primed bursts during naturalistic viewing (Figure 2). To quantify the relationship between visually evoked hyperpolarization and firing mode, we made spike-triggered averages (STAs) of the neural responses that preceded tonic spikes (tSTA) or the first spike in a burst (bSTA) (Lu et al., 1992). There were stereotyped differences between the averages computed for tonic and burst spikes as exemplified by two cells, one for which we recorded the membrane voltage (Figure 4A), and the other for which we recorded the membrane current (Figure 4B). Specifically, there was a sustained hyperpolarization, or outward current, before burst spikes, whereas a brief depolarization, or inward current, preceded tonic spikes (Figures 4A and 4B). This difference was easily seen when spikes and EPSCs were subtracted from the averaged currents that preceded either burst or tonic events and the two resulting signals were overlaid (Figure 5C). A further analysis of the difference between the shape of the pull that precedes tonic spikes with long interspike intervals versus bursts is provided in the Supplement; see Figure S2.

We quantified the membrane deflections preceding bursts and tonic spikes by fitting the time courses of the STAs (see Experimental Procedures). The times to reach half-maximal amplitude for the inhibition that preceded bursts were  $250.0 \pm 28.0$  ms ( $n = 12$ ) for membrane voltage and  $248.7 \pm 18.7$  ms ( $n = 22$ ) for membrane current. The times to reach half-maximal amplitude for the excitation preceding tonic spikes was  $39.3 \pm 10.6$  ms ( $n = 12$ ) for membrane voltage and  $36.7 \pm 8.2$  ms ( $n = 22$ ) for membrane current. There were minor differences among X, Y, and W cells (Figure 4C), but the general pattern of response was the same.

(G) Responses to defined suppressive stimuli. Individual responses to a bright disk flashed in the center of the receptive field of an Off cell are shown in black above the average of 20 trials in gray. Bursts followed withdrawal of the stimulus (red asterisks). Horizontal bars mark stimulus duration; the stimulus size was  $1^\circ$ , and the scale bars are 100 pA and 100 ms.

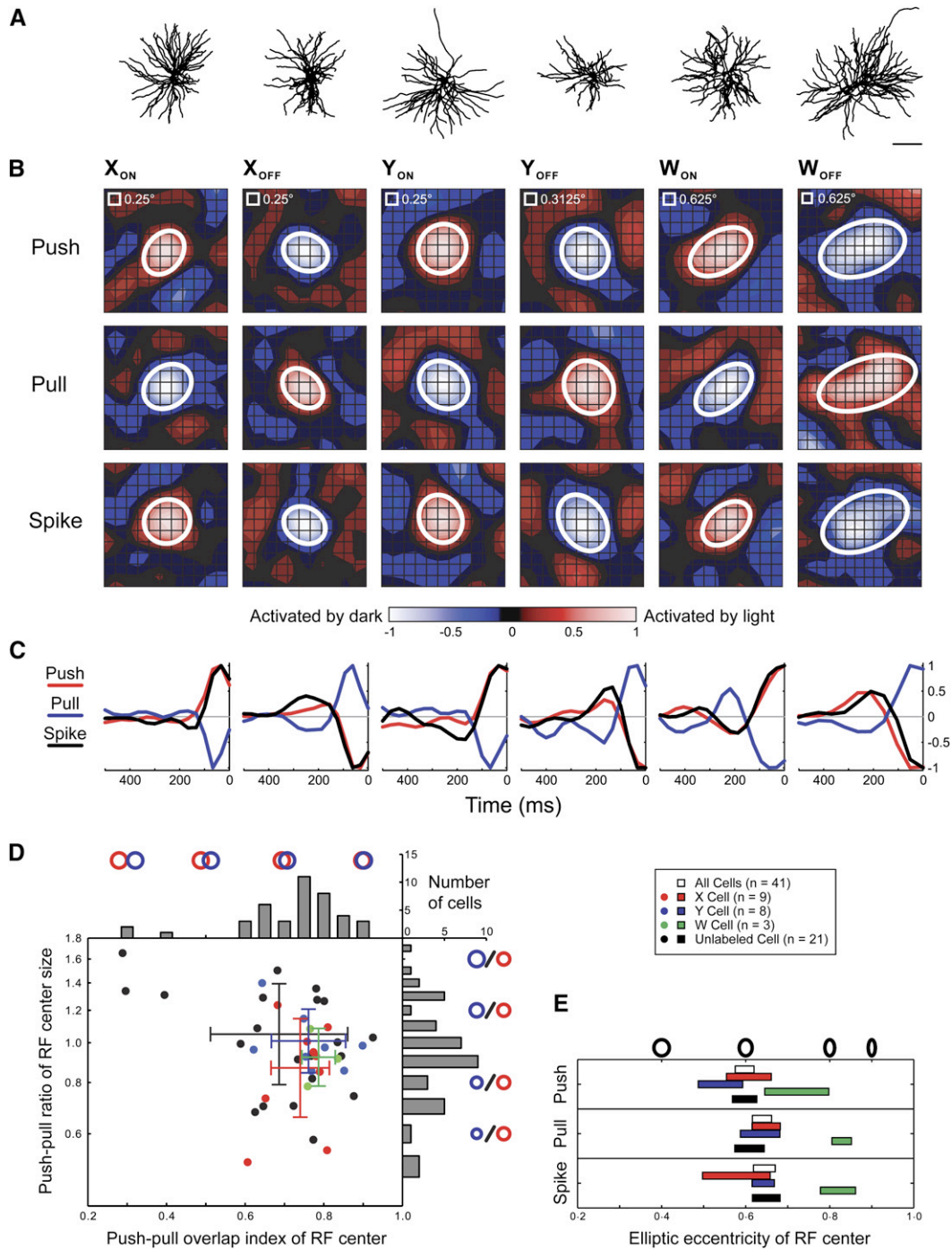


**Figure 3. Receptive Fields of Synaptic Excitation, or Push; Inhibition, or Pull; and Spikes Reconstructed with Natural Movies**

(A) Anatomical reconstruction of six relay cells. Anatomical class and center polarities are as labeled; scale bar, 100  $\mu$ m.

(B) Receptive fields of the push (top), the pull (middle), and spikes (bottom); white ellipses are  $1.5\sigma$  contours of 2D Gaussian fits of the centers.

(C) Time course of the responses.

(D) Scatter plot of the overlap index versus the ratio of sizes of the push to the pull. Histograms of the distributions of the overlap index (top) and the ratio of sizes (right) are shown next to graphical depictions of the two measures; crosses outline the mean  $\pm$  standard deviation.

(E) Elliptic eccentricities of the receptive field centers of push, pull, and spikes; horizontal bars indicate the mean  $\pm$  SEM. Values for X cells are in red; Y cells, in blue; W cells, in green; and remaining unlabeled cells, in black.

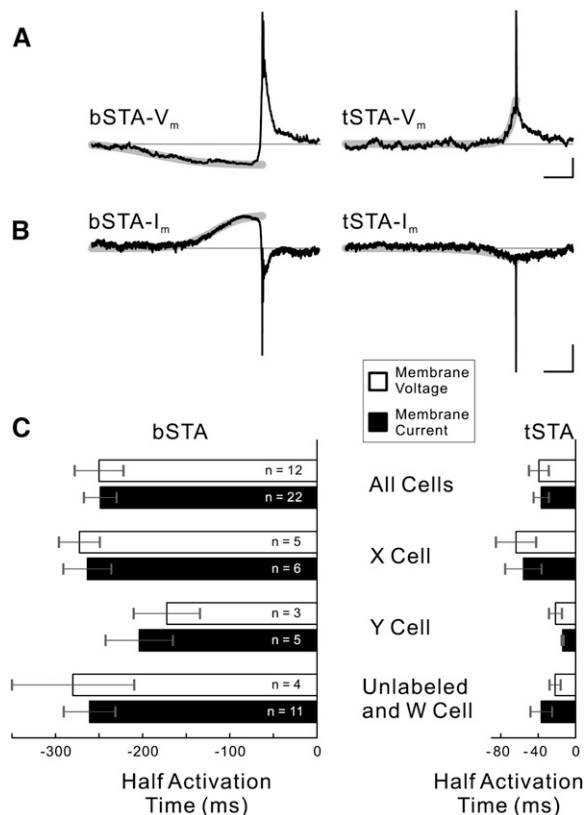


**Figure 4. Pull from the Center of the Receptive Field Precedes Bursts, but Not Tonic Spikes, Evoked by Natural Movies**

(A and B) Burst (bSTA) and tonic (tSTA) spike-triggered averages of membrane current ( $I_m$ ) and voltage ( $V_m$ ) of two relay cells (black traces). Sigmoid fit of bSTA and single exponential fit of tSTA (gray bands) was used. Scale bars are 100 ms and 2mV in (A), and 100 ms and 25 pA in (B).

(C) Time courses of the hyperpolarization, or outward currents, and depolarization, or inward currents, preceding burst versus tonic spikes. Values for membrane currents are shown in white and membrane voltage in black for different cell types as indicated. Error bars show mean  $\pm$  SEM.

To illustrate further the link between feedforward inhibition and the generation of bursts, we first ensured that the spatiotemporal receptive field constructed from the neural signal (Figure 5A) was able to predict the visually evoked pull (Figure 5B). Next, we built a simple model to show how the pull signal recorded in response to one movie can predict the occurrence of bursts evoked in response to a different movie. To construct the model, we extracted the waveform of the pull response in a 500 ms time window before each tonic or burst spike (Figure 5C), and then used principal component analysis to capture the structure of the pull (Figure 5D). The waveforms preceding tonic and burst spikes formed two displaced distributions in the space spanned by the first two principle components, with the tSTA and the bSTA as centers-of-mass of the distributions (Figure 5D). To classify the different shapes of the pull that precedes tonic versus burst spikes,

we projected the data onto a line (green arrow in Figures 5D and 5E) that connected the tSTA and the bSTA and then selected a simple criterion with a fixed arbitrary threshold on this axis (blue line in Figure 5E). The model predicted the occurrence of the bursts quite well (Figures 5F and 5G). First, receiver operating characteristic (ROC) analysis (black curve in Figure 5F) shows that the model correctly classified most bursts and gave few false positives for a wide range of thresholds. Second, we generated a new ROC curve (gray curve in Figure 5F) made by testing the model with a surrogate dataset produced with a bootstrap procedure (1000 iterations) that randomized the temporal relationship between the pull and the spike trains. The 95% confidence intervals for the surrogate data set lie far from the original ROC curve, showing that the model's performance is statistically significant.

Taken together, our results suggest that bursts are primed by feedforward inhibition, presumably mediated via local interneurons. That is, bursts are preceded by lasting periods of hyperpolarizing input, and the receptive fields reconstructed from these hyperpolarizations have the shape of retinal input.

#### Feedforward Excitation Initiates Thalamic Bursts

There are two simple possibilities that could account for the mechanism that triggers bursts: intrinsic regenerative currents that are activated by prolonged hyperpolarization (e.g., the anode break response) or synaptic excitation. We examined possible synaptic contributions by computing cross-correlations between retinal synaptic events and putative T-currents (Figure 6A) and between putative T-currents and the first spike of the burst (Figure 6B). We performed this analysis on the population rather than on single cells because the mean burst rate was low, 0.32 Hz, compared with 11.4 Hz for all spikes (recall that the putative T-currents were obtained from the trace that remained after spikes and EPSCs were extracted from the raw data; Figure 2F, asterisk). The stimulus-dependent correlations in the response were removed by subtracting the shift predictor (Perkel et al., 1967). The correlograms were standardized by dividing the event count within each bin by the total event count and the bin width, which is approximately equivalent to calculating the conditional probability density of two types of event, either  $p(t; \text{T-current}|\text{EPSC})$  (Figure 6A) or  $p(t; \text{burst}|\text{T-current})$  (Figure 6B). The analysis suggests that bursts were initiated by T-currents that, themselves, were evoked by retinal input. That is, the tall peak between 0 and 12 ms in the correlogram for T-current to EPSC (Figure 6A) indicated that T-currents were most likely to occur just after retinal input. There was a similar relationship between the onset of a T-current and the first spike of a burst (Figure 6B).

To tie together the relationship between retinal inputs and bursts, we computed the correlogram between each burst and the EPSC that preceded it most directly (Figure 6C). In this figure, we plot both the raw correlogram (solid line) and the shift predictor (dashed line). This plot reveals a close temporal relationship (0–8 ms) between the

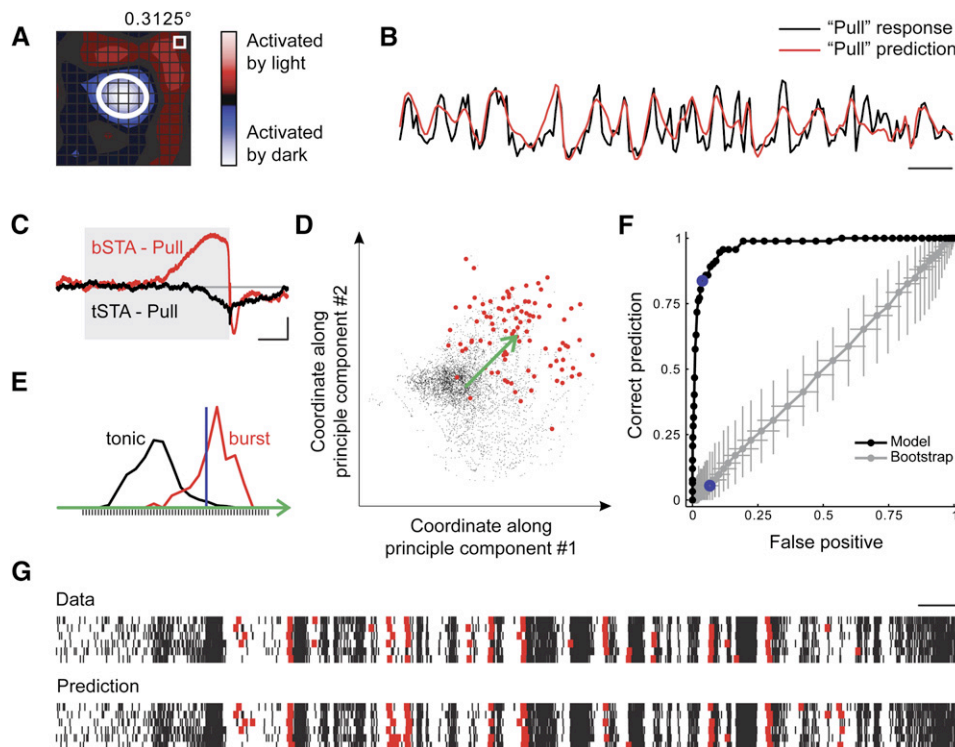


**Figure 5. Model Prediction of the Occurrence of Burst and Tonic Spikes Based on Feedforward Synaptic Inhibition**

(A) Receptive field of synaptic inhibition reconstructed for the cell in Figure 4B. (B) Predicted response of the pull by the receptive field (red) overlaid with the actual pull response (black); scale bar is 1 s. (C) bSTA (red) and tSTA (black) of the pull for the cell in Figure 4B; gray shades a 500 ms time window before the occurrence of spikes. Scale bars are 100 ms and 10 pA. (D) Scatter plot of the second versus first principal components of the pull waveform in a 500 ms window before tonic (black dots) and burst (red dots) spikes. Green arrow represents the vector linking the tSTA to the bSTA. (E) Distribution of tonic (black) and burst (red) events along the tSTA-bSTA axis; black ticks mark the different threshold levels used to generate receiver operating characteristic (ROC) curves in (F), and the blue line shows the threshold level used to predict event identity in (G). (F) ROC curves of the model's performance on another movie (black) and for bootstrap resampling (gray). Dots represent different threshold levels. Gray lines mark the 95% bootstrap confidence interval, and the filled blue circle marks the threshold level used in (G). (G) Prediction of spike type (tonic or burst) based on the inhibitory waveforms taken from responses to another movie; thick red lines represent bursts. Scale bar is 1 s. Note that the model produces serial bursts because it does not include a refractory period.

triggering EPSC and the first burst spike. Most importantly, the plot addresses the question of how many of the bursts and T-currents were initiated by retinal drive. In other words, it illustrates the contribution (Levick et al., 1972), or estimate of the percentage of cases in which a burst was initiated by retinal input; the maximum possible value is 1.0. For our sample, the contribution was high (0.8), as measured by integrating the 0–8 ms peak of the correlogram (shaded region). Similarly high values for the contribution of EPSCs to T-currents and T-currents to bursts were found in all populations of cells (Figure 6D). Insets below illustrate examples of the sequence of EPSC, putative T-current, and burst for an X, a Y, and a W cell (Figure 6E).

## DISCUSSION

We asked if synaptic inputs evoked by natural visual stimuli are able to induce both burst and tonic modes of firing in relay cells. First, we investigated the synaptic structure

of the relay cell's receptive field with simple stimuli and found a push-pull arrangement in both center and surround; that is, excitation from the retina was complemented by strong inhibition evoked by stimuli of the opposite sign. Second, we found that responses to natural movies were composed of two main patterns of response, either trains of excitatory synaptic events that elicited tonic spikes or inhibitory periods followed by bursts. Third, we reconstructed the receptive fields of synaptic inputs evoked by the movies and observed that the inhibition that preceded bursting came mainly from the central sub-region. The shape of the inhibitory field always matched the shape of excitatory fields reconstructed from retinal inputs, suggesting that it is made by feedforward circuits (Figure 1D). Finally, the bursts themselves were initiated by direct retinal input rather than intrinsic membrane properties. Thus, natural stimuli evoke sequences of inhibition and excitation that engage dual modes of activity in the thalamus.

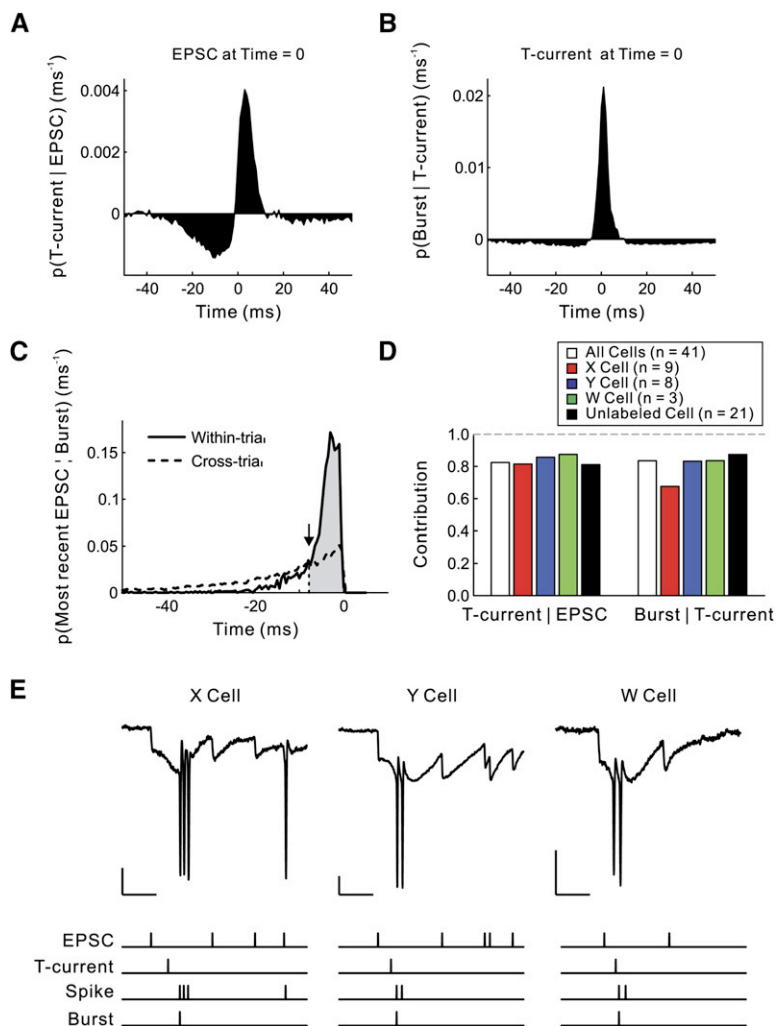


**Figure 6. Retinogeniculate Synaptic Inputs Trigger Putative T-Currents that Evoke Bursts**

(A) Cross-correlogram of putative T-currents with EPSCs (EPSC at  $t = 0$ ). The shift predictor has been subtracted from the raw correlogram; bin width, 1.0 ms;  $n = 41$ .

(B) Cross-correlogram of the first spikes in bursts with the putative T-currents (T-current at  $t = 0$ ); conventions and sample size as in (A).

(C) Conditional probability densities of the interval between a burst and most recent retinal EPSC (EPSC at  $t = 0$ ); time bin, 0.5 ms. Within-trial (solid line) and cross-trial (dashed line) probability densities intercept at about 8 ms (arrow); the contribution value, i.e. the shaded area, is 0.80 in this case;  $n = 41$ .

(D) Contribution values calculated for retinal inputs to putative T-currents and putative T-currents to bursts for intervals of 0 to 12 ms and  $-5$  to 10 ms, respectively.

(E) Examples of retinal inputs that trigger T-currents that initiate bursts in turn; scale bars, 50 pA and 20 ms.

A great deal of evidence suggests that retinal (feedforward) input rather than cortical (feedback) input determines the shape of the thalamic receptive fields. For example, the receptive fields of relay cells have the same outline as those of their strongest retinal inputs (Cleland et al., 1971; Levick et al., 1972; Usrey et al., 1999) and change only modestly after cortical feedback is removed (Cudeiro and Sillito, 1996). The two sources of inhibitory input to the lateral geniculate nucleus, local intranuclear interneurons and neurons in the overlying perigeniculate nucleus, have very different receptive fields. Specifically, there is evidence that local interneurons have discrete center-surround receptive fields (Dubin and Cleland, 1977; Humphrey and Weller, 1988; Sherman and Friedlander, 1988), whereas most neurons in the perigeniculate have large amorphous receptive fields in which bright and dark stimuli are excitatory throughout (Uhrich et al., 1991; Wörgötter et al., 1998); see Figure 1D.

Because we recorded intracellularly, we were able to measure the inhibitory as well as the excitatory contributions to the relay cell's receptive field. We found strong

push-pull in both the center and surround, consistent with earlier pharmacological (Sillito and Kemp, 1983) and intracellular (Martinez et al., 2005; McIlwain and Creutzfeldt, 1967; Singer and Creutzfeldt, 1970) studies. Large annular shapes evoked the strongest response from the surround, whereas stimuli like disk movies or noise did so for the center. The receptive fields mapped from noise or movies were similar, even though the reconstructions of the receptive field captured only the linear component of the response, which, as expected (Dan et al., 1996; Mante et al., 2005), accounted for more than half of the variance of the responses we recorded.

The dominant pull in the relay cell's receptive field appears to be fed forward from retina via local interneurons because its spatial structure resembled that of retinal receptive fields rather than the receptive fields of cells in the perigeniculate nucleus. This inhibition, when recruited by natural movies, was able to drive the membrane from tonic to burst mode. bSTAs showed that the inhibitory epochs that preceded bursts typically lasted for hundreds of milliseconds, long enough to deinactivate T-channels

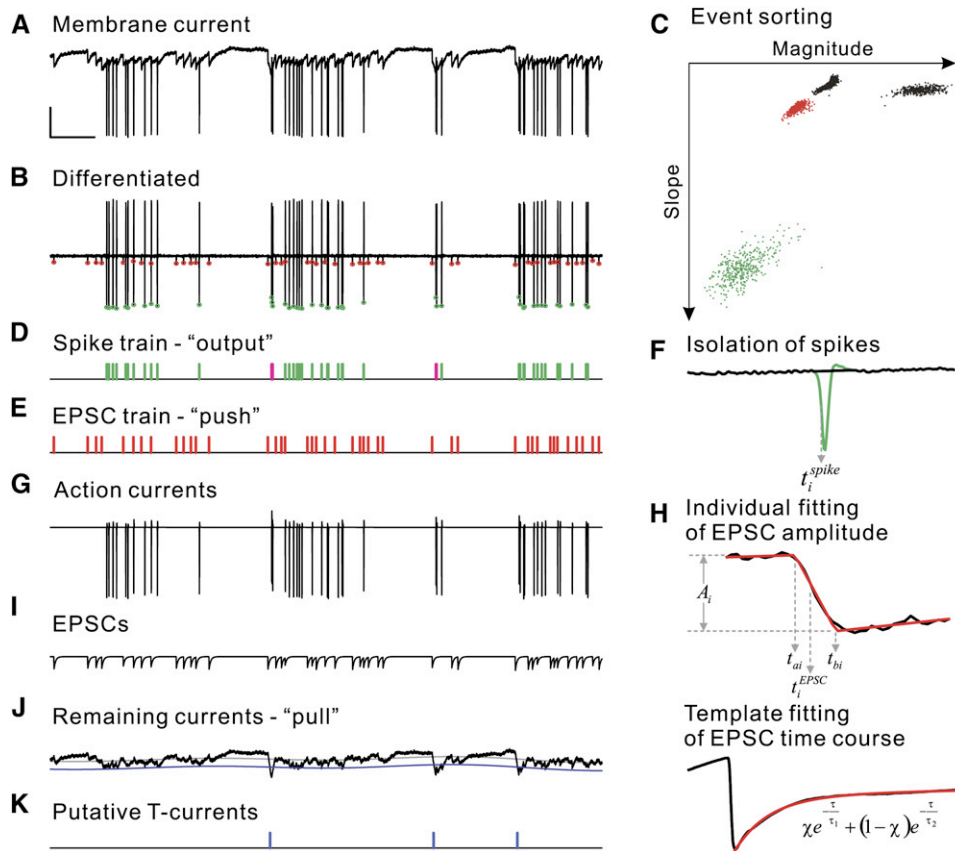


**Figure 7. Extraction of Neural Events and Components from Voltage-Damped Recordings**

- (A) Raw recording of membrane current.  
 (B) The same signal smoothed and differentiated; all local minima were used as candidate neural events. Events ultimately classified as EPSCs are labeled with red, and those classified as spikes are labeled with green in this and remaining panels.  
 (C) Scatter plot of the candidate events plotted as peak value (slope in the raw signal) against area under the peak (magnitude in the raw signal).  
 (D) Trains of spike times including bursts (magenta).  
 (E) EPSC times.  
 (F) Illustration of spikes (action currents) isolated from the raw signal.  
 (G) Isolated action currents.  
 (H) Fitting the template to model EPSCs. Parameters are as they appear in Equation 1.  
 (I) Modeled EPSCs as the EPSC train convolved with the template.  
 (J) Residual currents remaining after subtraction of the action currents and modeled EPSCs; blue line indicates one-tenth spike height.  
 (K) Times of putative T-currents, defined as events that crossed and remained below the blue line for longer than 10 ms as in (H).  
 Scale bar, 50 pA and 200 ms for panels on the left.

(Jahnsen and Llinas, 1984; McCormick and Huguenard, 1992; Soltesz et al., 1989). By contrast, tonic spikes were preceded by brief depolarizations. For almost all bursts we recorded, the underlying slow depolarizations (the putative T-currents) were initiated by excitatory synaptic events. Thus, natural movies typically evoke bursts that are primed by prolonged inhibition, but initiated by retinal drive.

Although bursts usually occurred at the end of a hyperpolarizing interval, we occasionally observed cases in which they were produced by a single excitatory event that arrived in the midst of prolonged inhibition. We also found that many putative T-currents were not large enough to drive the membrane across the threshold for

sodium spikes or led to only one sodium spike. This variability in the appearance and action of T-currents recalls a recent study in vitro that showed that the effects of these currents change depending on the level of background synaptic activity in both hyperpolarized and depolarized regimes (Wolfart et al., 2005). Apparently, synaptic interactions with T-channels have diverse effects on firing, with bursting the most stereotyped case.

Our study illustrates the importance of the receptive field in influencing firing mode. Naturalistic stimuli cause the generation of bursts in response to marked changes in luminance within the center of the receptive field. Thus, the pull within the receptive field is not only able to suppress firing, but also able to heighten the response

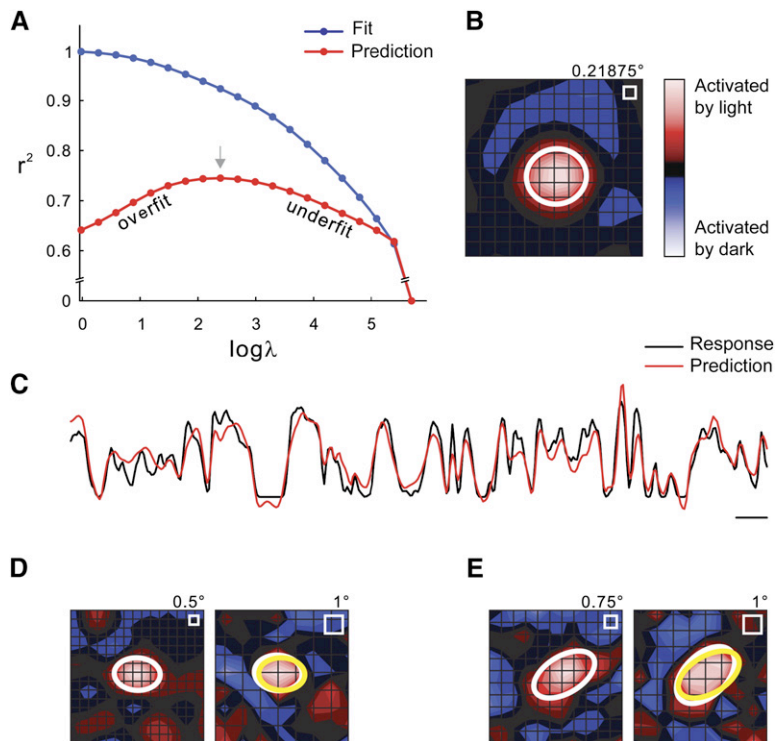


**Figure 8. Explanation and Controls for Receptive Field Reconstruction**

(A) Fraction of explained variance by the fitted response (blue) and the predicted response (red) as a function of  $\lambda$ , the Lagrange multiplier for regularization (Equation 4); prediction is made with a different movie.

(B) The kernel that best predicted the receptive field was chosen as the reconstructed receptive field (indicated by the gray arrow in A).

(C) Predicted response (red) by the optimized kernel overlaid with the actual response (black); scale bar, 500 ms.

(D and E) Side-by-side comparisons of receptive fields reconstructed from responses to movies (left) and receptive fields mapped with sparse noise (right). White ellipses are  $1.5\sigma$  contours of 2D Gaussian fits of the centers; yellow ellipses replicate the white ones in the panels to the left.

to changes in stimulus polarity. This was common to all types of relay cells in all layers of the lateral geniculate. Thus, our results are consistent with extracellular (Alitto et al., 2005; Denning and Reinagel, 2005) and theoretical (Lesica and Stanley, 2004) studies that conclude that bursts signal transitions from periods of lasting brightness or darkness.

Somewhat similar interactions between inhibition and firing mode might operate at the level of retina since ganglion cells have T-channels (Lee et al., 2003) and receptive fields with push-pull (Wiesel, 1959). In fact, based on extracellular analyses of the thalamus, it had been proposed that every spike in a thalamic burst is generated by a corresponding presynaptic retinal input (Sincich et al., 2007). Intracellular recordings do not support the view that thalamic bursts depend exclusively on presynaptic mechanisms, however. The frequency of visually evoked bursts increases when the membrane voltage of the postsynaptic relay cell is lowered by current injection (see Figure S1 and Lu et al., 1992). Moreover, this increase significantly exceeds the number of bursts that the retina generates (see Figure S4 for complete analysis).

Although our experiments were performed in anesthetized animals, our recordings were made when the membrane rested in tonic mode. In that state, natural movies evoked bursts infrequently but predictably, reminiscent of patterns observed in awake animals (Guido and Weyand, 1995; Ramcharan et al., 2000; Swadlow and Gusev, 2001; Weyand et al., 2001). This sparseness of occurrence does not mean that bursts are unimportant. Bursts might be used to provide a history of changes in the visual

environment and to signal rare events that (perhaps because they are rare) are especially important to notice (Alitto et al., 2005; Denning and Reinagel, 2005; Lesica and Stanley, 2004; Lesica et al., 2006). Thus, it seems that evolutionary pressures favored the use of the same membrane channels in both sleep and wakefulness.

## EXPERIMENTAL PROCEDURES

### Extraction of Synaptic Currents in the Intracellular Membrane Current

#### Preparation, Stimulation, and Recordings

Anesthetized adult cats (1.5–3.5 kg) were prepared as described earlier (Hirsch et al., 1998), except that anesthesia was induced with propofol and sufentanil (20 mg/kg + 1.5  $\mu$ g/kg, i.v.) and maintained with propofol and sufentanil (5  $\mu$ g/kg/hr + 1.5  $\mu$ g/kg/hr, i.v.). All procedures were in accordance with the guidelines of the National Institute of Health and the Institutional Animal Care and Use Committee of the University of Southern California. Whole-cell recordings with dye-filled pipettes were made using standard techniques (Hirsch et al., 1998) (Axopatch 200A amplifier, Axon Instruments, Inc., Union City, CA), digitized at 10 kHz (Power1401 data acquisition system, Cambridge Electronic Design, Ltd., Cambridge, UK), and stored for further analysis. It was often impractical to assign absolute resting voltage since the ratio of access to seal resistance led to a voltage division in the neural signal (Martinez et al., 2005). Following histology, cells were identified as X, Y, or W using criteria outlined in Friedlander et al., 1981 and Humphrey and Weller, 1988.

The stimuli, natural movies, sparse (Hirsch et al., 1998) and 2D Gaussian noise, and discs and annuli were displayed at 19–50 frames per second on a computer monitor (refresh rate 128–160 Hz) by means of a stimulus generator (Vsg2/5 or ViSaGe, Cambridge Research Design, Ltd., Cambridge, UK). In some instances the movies were shown through an aperture in a uniform mask set to mean luminance.

### EPSCs and Spikes

Intracellular voltage-damped signals (Figure 7A) were digitally filtered (Gaussian filter, 0.5 ms bandwidth) and then differentiated twice to identify spikes and EPSCs (Figure 7B). Potential spikes and synaptic events were characterized as concave local minima (zero crossing of the first derivative with a negative second derivative). Event times for spikes  $\{t_i^{spike}\}$  and EPSCs  $\{t_i^{EPSC}\}$  were identified from the set of potential events by plotting amplitude (the area under the peak of the first derivative) against slope (the peak value of the first derivative). That is, the spikes and EPSCs formed distinct clusters in this plot and could be separated from each other and from noise by means of a threshold criterion (Figure 7C). Sometimes EPSCs split into multiple clusters, indicating the presence of different inputs; in these instances we combined all the clusters of EPSCs that were separable from noise into one group for further analysis.

### IPSCs

IPSCs could not be resolved individually and were visible only as slow outward currents. Our strategy to isolate these currents was to subtract spikes and EPSCs from the total membrane current. We eliminated spikes by removing the data points from the raw signal at each  $t_i^{spike}$  within a window of  $-0.5$  to  $1.5$  ms and then closing the gaps by cubic interpolation (Figure 7F). EPSCs were less simple to remove since their size varied and their long time courses lead to frequent overlap. Thus, we modeled individual EPSCs by a linear-exponential-decay function:

$$\sigma_i^{EPSC}(\tau; A_i, t_{bi}, t_{di}, \chi, \tau_1, \tau_2) = \begin{cases} 0 & (\tau < t_{bi}) \\ A_i \frac{(\tau - t_{bi})}{t_{di} - t_{bi}} & (t_{bi} \leq \tau \leq t_{di}) \\ A_i \left[ \chi e^{-\frac{\tau}{\tau_1}} + (1 - \chi) e^{-\frac{\tau}{\tau_2}} \right] & (\tau > t_{di}) \end{cases} \quad (1)$$

The EPSC template was fitted in two steps: first, the linear rise of the template was fitted to the EPSC onset ( $-1.5$  to  $2.5$  ms window around each  $t_i^{EPSC}$ ) to determine the amplitude  $A_i$  (Figure 7H, upper trace). Second, the exponential decay was fitted to the EPSC-triggered-average of membrane current that followed the onset of the EPSC (Figure 7H, lower trace). The current that remained after removing spikes (Figure 7G) and EPSCs (Figure 7I) was a slow outward current (Figure 7J) containing mainly IPSCs but including other rare features such as the putative T-currents. This current was used to map the pull.

For two cells, we cross-checked this method of extracting the pull signal by subtracting a recording made at a hyperpolarized voltage from one made at a depolarized voltage (hyperpolarization reduces the amplitude of synaptic inhibition). The receptive fields obtained from both methods were similar. For almost all cells, as a separate control, we compared the receptive fields reconstructed from the movies with those made by averaging responses to the noise stimuli; the fields were always similar.

### Putative T-Currents

First, the signal was high-pass filtered at  $1.0$  Hz to remove slow artifactual drift in the signal. Putative T-currents were detected in the pull currents by using a threshold criterion; inward deflections were counted as putative T-currents if their amplitude exceeded one-tenth average action current height for more than  $10$  ms (Figure 7J). The onsets were defined as the time the signal crossed threshold (Figure 7K).

### tSTA and bSTA

#### Identification of Tonic and Burst Spikes

Bursts were defined by criteria used in intracellular studies since these standards hold up well for intracellular recordings (Ramcharan et al., 2000). Specifically, bursts were defined as events that comprised two or more spikes spaced less than  $4$  ms apart and in which the first spike of the rapid train occurred no less than  $100$  ms after the most recent spike. The start of each burst was taken to be the timing of its first spike.

### STA of Membrane Current and Voltage

The cross-correlogram of membrane current/voltage to burst and tonic spikes was generated by event-triggered averaging. In recordings with a sufficient number of events, the cross-correlogram to burst events was fitted well by a sigmoid:

$$f(\tau) = \frac{\alpha}{1 + \exp[\beta(\tau - \tau_{1/2})]} \quad (2)$$

and the cross-correlogram to tonic events was fitted well with a single exponential:

$$f(\tau) = \alpha \cdot 2^{-\tau/\tau_{1/2}} \quad (3)$$

where  $\tau_{1/2}$  was used to quantify the time course in both cases. For many cells, the cross-correlograms for bursts were very noisy because bursts occurred at low frequency (mean,  $0.32$  Hz,  $n = 41$ ). Our criterion for including cross-correlograms for further analysis was that the correlation coefficient with the fitting function satisfied  $r^2 > 0.75$ .

### Reconstruction of Spatiotemporal Receptive Field

Spatiotemporal receptive fields were estimated from responses to natural movies by optimizing a linear convolution model for predicting responses to the stimulus. Firing rates of EPSCs and spikes were estimated by a temporal Gaussian filter ( $25$  ms half-width). Since the pull signal was analog versus digital-like spikes or EPSCs, we estimated the pull by averaging the membrane currents in each frame of the movie. Spontaneous (stimulus-independent) response levels were estimated by averaging responses over the entire recording.

The receptive fields were estimated as the linear convolution kernels that minimized the quadratic error between predicted and measured responses. For optimization we used a regularized gradient method (Machens et al., 2004). The kernel, stimulus, and response were discretized in space and time. The spatial bin was determined according to the size of the receptive field (bin size, range  $0.125^\circ$  to  $1.0^\circ$ ), and the temporal bin was set to the duration of a movie frame (bin size, range  $20.0$  to  $52.6$  ms). The total duration of the kernel was set to  $600$  or  $800$  ms. The 3D kernel was reshaped into a 1D vector  $\mathbf{h}$ , and similarly, the stimulus into a matrix,  $\mathbf{S}$ . The optimization function is then given as a quadratic form:

$$E = \frac{1}{2}(\mathbf{S} \cdot \mathbf{h} - \mathbf{r})^T (\mathbf{S} \cdot \mathbf{h} - \mathbf{r}) + \frac{\lambda}{2}(\mathbf{R} \cdot \mathbf{h})^T (\mathbf{R} \cdot \mathbf{h}) \quad (4)$$

with the first term the prediction error and the second a regularization term for avoiding overfitting (because of the limited amount of data,  $\mathbf{S}$  usually has more columns than rows). The regularizer  $\mathbf{R}$  smoothed the kernel by taking differences of immediate neighbors in all three dimensions (two spatial and one temporal).

We used a faster conjugate gradient algorithm than that used in earlier methods (Machens et al., 2004) to find the minimum. The minimization procedure was initialized with a random kernel and a Lagrange multiplier  $\lambda$  for regularization that was set to a large value. After each optimization step using the conjugate gradient algorithm,  $\lambda$  was reduced in a stepwise fashion with a power-law decay (Figure 8A). The decay parameter for  $\lambda$  was made small enough to prevent trapping in local minima. The annealing process ended when  $\lambda$  reached an empirical value that we determined from a case with sufficient data for cross-validation (Figure 8A, gray arrow); this value of  $\lambda$  was the one that minimized the prediction error of the response to a different movie stimulus. Convergence was verified by using different initializations. Centers of reconstructed receptive fields from natural movies by means of this approach agree with "sparse noise" maps reasonably well (Figure 8D and 8E).

Reconstructed receptive fields were normalized to absolute peak value. To obtain the spatial component of the receptive field, we integrated the time frames within the peak of the impulse response for the

center pixel. Temporal receptive fields were estimated by spatial integration of the spatiotemporal receptive field weighted by the Gaussian fit of the spatial receptive field center. The spatial receptive fields in the figures were plotted as cubic-smoothed contour-plots (MatLab, The MathWorks, Inc., Natick, MA).

### Quantification of Receptive Field Properties

#### Gaussian Fit of the Center

The spatial centers of receptive fields were fitted with Gaussians, and the fit parameters were used to represent receptive field properties. Each receptive field was first rectified to its center polarity and fitted by a 2D Gaussian with amplitude  $\alpha$ , spatial widths  $\sigma_a$  and  $\sigma_b$ , rotation angle  $\theta$ , and center position  $x_0$  and  $y_0$  (least-mean-square fit using the Nelder-Mead simplex algorithm, function *fminsearch*, MatLab).

#### Elliptic Eccentricity

We chose  $\sigma_a \geq \sigma_b$  and defined the elliptic eccentricity as

$$e = \sigma_a (\sigma_a^2 + \sigma_b^2)^{-1/2} \in [0, 1]$$

as a measure for the degree of elongation of the receptive field.

#### Overlap Index

To quantify the extent to which two spatial receptive fields overlap, Schiller's overlap index (Schiller et al., 1976) was extended to two dimensions: for two receptive fields with the Gaussian parameters  $(\alpha_1, \sigma_{a1}, \sigma_{b1}, \theta_1, x_{01}, y_{01})$  and  $(\alpha_2, \sigma_{a2}, \sigma_{b2}, \theta_2, x_{02}, y_{02})$ , the 2D overlap index was defined by

$$\Omega = \frac{\sigma_{12} + \sigma_{21} - d}{\sigma_{12} + \sigma_{21} + d} \quad (5)$$

where

$$\sigma_{ij} = \frac{\sigma_{a1}\sigma_{b1}}{\sqrt{\sigma_{a1}^2 \sin^2(\theta_1 - \phi_{ij}) + \sigma_{b1}^2 \cos^2(\theta_1 - \phi_{ij})}}$$

and  $([i,j] = [1,2] \text{ or } [2,1])$  are the widths of the two Gaussians along the direction linking their centers, with

$$\phi_{ij} = \arctan\left(\frac{y_{0j} - y_{0i}}{x_{0j} - x_{0i}}\right)$$

and  $d$  as the Euclidian distance between the centers.

#### Receptive Field Size

To compare sizes of two receptive fields, we used the ratio of the areas within the  $1/e$  contour:

$$\frac{A_2}{A_1} = \frac{\sigma_{a2}\sigma_{b2}}{\sigma_{a1}\sigma_{b1}} \quad (6)$$

### Cross-Correlation and Estimation of Contribution

The cross-correlograms of two discrete event trains were plotted as conditional probability density functions approximated by frequency histograms of conditional occurrence of one event at various temporal distances from the other. To compensate for stimulus-driven correlations, we generated shift predictors by forming cross-correlograms of shuffled trials (Perkel et al., 1967). The contribution of events A in triggering events B was defined as the fraction of all events B preceded by positively correlated events A (cross-correlation larger than shift-predictor, i.e., inside the peak of correlogram) (Levick et al., 1972; Usrey et al., 1999).

### Supplemental Data

The Supplemental Data for this article can be found online at <http://www.neuron.org/cgi/content/full/55/3/465/DC1/>.

### ACKNOWLEDGMENTS

We are grateful to L.M. Martinez, B.W. Mel, and C. Soto Sanchez for comments on the manuscript, and to C.M. Gray and J. Baker for contributing several of the movies we used. We thank J.M. Provost, C. Pili-lai, S.X.X. Xing, and B. Gary for reconstructing the labeled neurons. This work was supported by National Institutes of Health EY09593 (J.A.H) and the Redwood Center for Theoretical Neuroscience (F.T.S and K.K).

Received: April 27, 2007

Revised: June 14, 2007

Accepted: June 29, 2007

Published: August 1, 2007

### REFERENCES

- Allitto, H.J., Weyand, T.G., and Usrey, W.M. (2005). Distinct properties of stimulus-evoked bursts in the lateral geniculate nucleus. *J. Neurosci.* 25, 514–523.
- Blitz, D.M., and Regehr, W.G. (2003). Retinogeniculate synaptic properties controlling spike number and timing in relay neurons. *J. Neurophysiol.* 90, 2438–2450.
- Cleland, B.G., Dubin, M.W., and Levick, W.R. (1971). Simultaneous recording of input and output of lateral geniculate neurones. *Nat. New Biol.* 237, 191–192.
- Crunelli, V., Haby, M., Jassik-Gerschenfeld, D., Leresche, N., and Pirchio, M. (1988).  $\text{Cl}^-$  and  $\text{K}^+$ -dependent inhibitory postsynaptic potentials evoked by interneurons of the rat lateral geniculate nucleus. *J. Physiol.* 399, 153–176.
- Cudeiro, J., and Sillito, A.M. (1996). Spatial frequency tuning of orientation-discontinuity-sensitive corticofugal feedback to the cat lateral geniculate nucleus. *J. Physiol.* 490, 481–492.
- Dan, Y., Atick, J.J., and Reid, R.C. (1996). Efficient coding of natural scenes in the lateral geniculate nucleus: experimental test of a computational theory. *J. Neurosci.* 16, 3351–3362.
- Denning, K.S., and Reinagel, P. (2005). Visual control of burst priming in the anesthetized lateral geniculate nucleus. *J. Neurosci.* 25, 3531–3538.
- Dong, D.W., and Atick, J.J. (1995). Statistics of natural time-varying images. *Network: Comput. Neural. Syst.* 6, 345–358.
- Dubin, M.W., and Cleland, B.G. (1977). Organization of visual inputs to interneurons of lateral geniculate nucleus of the cat. *J. Neurophysiol.* 40, 410–427.
- Fourment, A., Hirsch, J.C., Marc, M.E., and Guidet, C. (1984). Modulation of postsynaptic activities of thalamic lateral geniculate neurons by spontaneous changes in number of retinal inputs in chronic cats. 1. Input-output relations. *Neuroscience* 12, 453–464.
- Friedlander, M.J., Lin, C.S., Stanford, L.R., and Sherman, S.M. (1981). Morphology of functionally identified neurons in lateral geniculate nucleus of the cat. *J. Neurophysiol.* 46, 80–129.
- Granseth, B., and Lindstrom, S. (2003). Unitary EPSCs of Corticogeniculate Fibers in the Rat Dorsal Lateral Geniculate Nucleus In Vitro. *J. Neurophysiol.* 89, 2952–2960.
- Guido, W., and Weyand, T. (1995). Burst responses in thalamic relay cells of the awake behaving cat. *J. Neurophysiol.* 74, 1782–1786.
- Guido, W., Lu, S.M., and Sherman, S.M. (1992). Relative contributions of burst and tonic responses to the receptive field properties of lateral geniculate neurons in the cat. *J. Neurophysiol.* 68, 2199–2211.
- Hamos, J.E., Van Horn, S.C., Raczkowski, D., and Sherman, S.M. (1987). Synaptic circuits involving an individual retinogeniculate axon in the cat. *J. Comp. Neurol.* 259, 165–192.

- Hirsch, J.A., Alonso, J.M., Reid, R.C., and Martinez, L.M. (1998). Synaptic integration in striate cortical simple cells. *J. Neurosci.* *18*, 9517–9528.
- Humphrey, A.L., and Weller, R.E. (1988). Structural correlates of functionally distinct X-cells in the lateral geniculate nucleus of the cat. *J. Comp. Neurol.* *268*, 448–468.
- Jahnson, H., and Llinas, R. (1984). Electrophysiological properties of guinea-pig thalamic neurones: an in vitro study. *J. Physiol.* *349*, 205–226.
- Lee, S.C., Hayashida, Y., and Ishida, A.T. (2003). Availability of low-threshold  $\text{Ca}^{2+}$  current in retinal ganglion cells. *J. Neurophysiol.* *90*, 3888–3901.
- Lesica, N.A., and Stanley, G.B. (2004). Encoding of natural scene movies by tonic and burst spikes in the lateral geniculate nucleus. *J. Neurosci.* *24*, 10731–10740.
- Lesica, N.A., Weng, C., Jin, J., Yeh, C.I., Alonso, J.M., and Stanley, G.B. (2006). Dynamic encoding of natural luminance sequences by LGN bursts. *PLoS Biol.* *4*, e209. 10.1371/journal.pbio.0040209.
- Levick, W.R., Cleland, B.G., and Dubin, M.W. (1972). Lateral geniculate neurons of cat: retinal inputs and physiology. *Invest. Ophthalmol.* *11*, 302–311.
- Liu, R.C., Tzonev, S., Rebrik, S., and Miller, K.D. (2001). Variability and information in a neural code of the cat lateral geniculate nucleus. *J. Neurophysiol.* *86*, 2789–2806.
- Livingstone, M.S., and Hubel, D.H. (1981). Effects of sleep and arousal on the processing of visual information in the cat. *Nature* *291*, 554–561.
- Lu, S.M., Guido, W., and Sherman, S.M. (1992). Effects of membrane voltage on receptive field properties of lateral geniculate neurons in the cat: contributions of the low-threshold  $\text{Ca}^{2+}$  conductance. *J. Neurophysiol.* *68*, 2185–2198.
- Machens, C.K., Wehr, M.S., and Zador, A.M. (2004). Linearity of cortical receptive fields measured with natural sounds. *J. Neurosci.* *24*, 1089–1100.
- Mante, V., Frazor, R.A., Bonin, V., Geisler, W.S., and Carandini, M. (2005). Independence of luminance and contrast in natural scenes and in the early visual system. *Nat. Neurosci.* *8*, 1690–1697.
- Martinez, L.M., Wang, Q., Reid, R.C., Pillai, C., Alonso, J.M., Sommer, F.T., and Hirsch, J.A. (2005). Receptive field structure varies with layer in the primary visual cortex. *Nat. Neurosci.* *8*, 372–379.
- McCormick, D.A., and Huguenard, J.R. (1992). A model of the electrophysiological properties of thalamocortical relay neurons. *J. Neurophysiol.* *68*, 1384–1400.
- Mollwain, J.T., and Creutzfeldt, O. (1967). Microelectrode study of synaptic excitation and inhibition in the lateral geniculate nucleus of the cat. *J. Neurophysiol.* *30*, 1–21.
- Peichl, L., and Wässle, H. (1983). The structural correlate of the receptive field centre of alpha ganglion cells in the cat retina. *J. Physiol.* *341*, 309–324.
- Perkel, D.H., Gerstein, G.L., and Moore, G.P. (1967). Neuronal spike trains and stochastic point processes. II. Simultaneous spike trains. *Biophys. J.* *7*, 419–440.
- Ramcharan, E.J., Gnadt, J.W., and Sherman, S.M. (2000). Burst and tonic firing in thalamic cells of unanesthetized, behaving monkeys. *Vis. Neurosci.* *17*, 55–62.
- Reinagel, P., and Reid, R.C. (2000). Temporal coding of visual information in the thalamus. *J. Neurosci.* *20*, 5392–5400.
- Reinagel, P., Godwin, D., Sherman, S.M., and Koch, C. (1999). Encoding of visual information by LGN bursts. *J. Neurophysiol.* *81*, 2558–2569.
- Schiller, P.H., Finlay, B.L., and Volman, S.F. (1976). Quantitative studies of single-cell properties in monkey striate cortex. I. Spatiotemporal organization of receptive fields. *J. Neurophysiol.* *39*, 1288–1319.
- Sherman, S.M., and Friedlander, M.J. (1988). Identification of X versus Y properties for interneurons in the A-laminae of the cat's lateral geniculate nucleus. *Exp. Brain Res.* *73*, 384–392.
- Sherman, S.M., and Guillery, R.W. (1996). Functional organization of thalamocortical relays. *J. Neurophysiol.* *76*, 1367–1395.
- Shou, T., Ruan, D., and Zhou, Y. (1986). The orientation bias of LGN neurons shows topographic relation to area centralis in the cat retina. *Exp. Brain Res.* *64*, 233–236.
- Sillito, A.M., and Kemp, J.A. (1983). The influence of GABAergic inhibitory processes on the receptive field structure of X and Y cells in cat dorsal lateral geniculate nucleus (dLGN). *Brain Res.* *277*, 63–77.
- Sincich, L.C., Adams, D.L., Economides, J.R., and Horton, J.C. (2007). Transmission of spike trains at the retinogeniculate synapse. *J. Neurosci.* *27*, 2683–2692.
- Singer, W., and Creutzfeldt, O.D. (1970). Reciprocal lateral inhibition of on- and off-center neurones in the lateral geniculate body of the cat. *Exp. Brain Res.* *10*, 311–330.
- Soltesz, I., Lightowler, S., Leresche, N., and Crunelli, V. (1989). Optic tract stimulation evokes GABAA but not GABAB IPSPs in the rat ventral lateral geniculate nucleus. *Brain Res.* *479*, 49–55.
- Steriade, M., McCormick, D.A., and Sejnowski, T.J. (1993). Thalamocortical oscillations in the sleeping and aroused brain. *Science* *262*, 679–685.
- Swadlow, H.A., and Gusev, A.G. (2001). The impact of 'bursting' thalamic impulses at a neocortical synapse. *Nat. Neurosci.* *4*, 402–408.
- Swadlow, H.A., Gusev, A.G., and Bezdudnaya, T. (2002). Activation of a cortical column by a thalamocortical impulse. *J. Neurosci.* *22*, 7766–7773.
- Uhlrich, D.J., Cucchiari, J.B., Humphrey, A.L., and Sherman, S.M. (1991). Morphology and axonal projection patterns of individual neurons in the cat perigeniculate nucleus. *J. Neurophysiol.* *65*, 1528–1541.
- Usrey, W.M., Reppas, J.B., and Reid, R.C. (1999). Specificity and strength of retinogeniculate connections. *J. Neurophysiol.* *82*, 3527–3540.
- Usrey, W.M., Alonso, J.M., and Reid, R.C. (2000). Synaptic interactions between thalamic inputs to simple cells in cat visual cortex. *J. Neurosci.* *20*, 5461–5467.
- Wässle, H., Boycott, B.B., and Illing, R.B. (1981). Morphology and mosaic of on- and off-beta cells in the cat retina and some functional considerations. *Proc. R. Soc. Lond. B. Biol. Sci.* *212*, 177–195.
- Weyand, T.G., Boudreaux, M., and Guido, W. (2001). Burst and tonic response modes in thalamic neurons during sleep and wakefulness. *J. Neurophysiol.* *85*, 1107–1118.
- Wiesel, T.N. (1959). Recording inhibition and excitation in the cat's retinal ganglion cells with intracellular electrodes. *Nature* *183*, 264–265.
- Wolfart, J., Debay, D., Le Masson, G., Destexhe, A., and Bal, T. (2005). Synaptic background activity controls spike transfer from thalamus to cortex. *Nat. Neurosci.* *8*, 1760–1767.
- Wörgötter, F., Nelle, E., Li, B., and Funke, K. (1998). The influence of corticofugal feedback on the temporal structure of visual responses of cat thalamic relay cells. *J. Physiol.* *509*, 797–815.